



HAL
open science

Design of a medium voltage power converter-storage devices embedded in a hybrid emergency network for more electrical aircraft

Rémy Rigo-Mariani, Fabien Lacressonniere, Guillaume Fontes, Xavier Roboam

► To cite this version:

Rémy Rigo-Mariani, Fabien Lacressonniere, Guillaume Fontes, Xavier Roboam. Design of a medium voltage power converter-storage devices embedded in a hybrid emergency network for more electrical aircraft. *Mathematics and Computers in Simulation*, 2013, 91, pp.72-90. 10.1016/j.matcom.2012.07.009 . hal-03286808

HAL Id: hal-03286808

<https://ut3-toulouseinp.hal.science/hal-03286808>

Submitted on 2 Feb 2022

HAL is a multi-disciplinary open access archive for the deposit and dissemination of scientific research documents, whether they are published or not. The documents may come from teaching and research institutions in France or abroad, or from public or private research centers.

L'archive ouverte pluridisciplinaire **HAL**, est destinée au dépôt et à la diffusion de documents scientifiques de niveau recherche, publiés ou non, émanant des établissements d'enseignement et de recherche français ou étrangers, des laboratoires publics ou privés.

Design of a medium voltage power converter-storage devices embedded in a hybrid emergency network for more electrical aircraft

R. Rigo Mariani^{*}, F. Lacressonniere, G. Fontes, X. Roboam

Université de Toulouse, LAPLACE (Laboratoire Plasma et Conversion d'Energie) UMR CNRS INPT UPS, ENSEEIHT, 2 rue Charles Camichel, BP 7122, F 31071 Toulouse Cedex 7, France

Abstract

The purpose of this paper is to present and describe a hybrid electrical network for an aircraft in emergency operation. The principle of this network is to hybridize, through a bidirectional DC/DC converter, a high speed turbine (Ram Air turbine – RAT) with an electrochemical storage. Some experiments on a lab test bench have allowed validating the principle of the hybridization and several energy management strategies have been tested with a low voltage lithium ion battery. A design study of DC/DC power converters, according to the voltage of that storage device, has been done. This study tries to be as exhaustive as possible in view of determining the best voltage connection in terms of mass and efficiency. This study has led to the design and sizing of a medium-voltage battery from which future tests will be carried out on the lab test bench.

© 2012 Published by Elsevier B.V. on behalf of IMACS.

Keywords: Power converter design; Electrical network; Hybridization; Energy management; Electrochemical storage

1. Introduction

The growth of air traffic over the past 20 years has been spectacular, and will continue in the future, particularly in the growing markets as in Asia. To limit the impact of the air traffic on the environment, the aircraft industry has to reduce the fuel consumption and CO₂ emissions of aircrafts [1]. The “more electric aircraft” can reach this environmental challenge [15,16].

The move to more electric aircraft will offer lower weight aircrafts with lower fuel burn. Indeed, the conventional equipments, which depend on hydraulic, pneumatic power, are substituted by several electrical systems such as flight control [15], anti ice systems, or air conditioning [19]. Yet, these substitutes mentioned have caused a considerable increase of the demand for electrical power in the aircraft [4,9,10,14,15]. Sometimes, some electrical storage devices could be implemented in the electrical network. For example, the application of a fuel cell system as an auxiliary power unit (APU) has many advantages as noise and CO₂ emissions reduction [11,13].

This paper deals with an emergency subnetwork in which energy generation is classically ensured by a RAT (Ram Air turbine) that unfolds in case of engine or electrical generation system failure. A recent study has demonstrated that a significant reduction could be expected in terms of weight and volume of that emergency subsystem (around

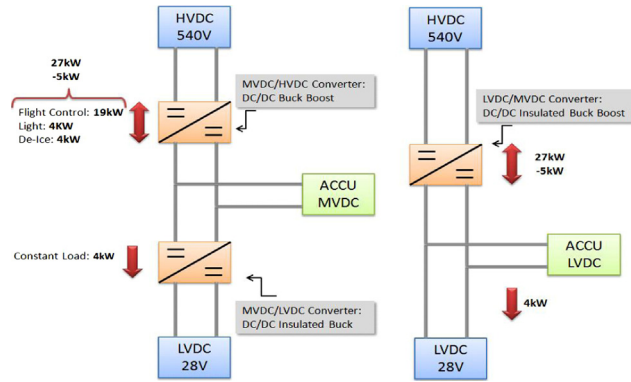


Fig. 1. Scheme of the considered network.

30%) by hybridizing the RAT with a storage device [10,14]. Hybridization is based on the principle of power sharing where the average power is supplied by the main power source (i.e. the RAT) while transient load is fed by the storage device. Thus several solutions such as supercapacitors [12], or batteries are considered as storage device which has to be connected to the electrical network. That connection is directly linked to the whole architecture of the considered network.

In this paper, the authors have to face a structure with two DC buses:

- A 540 V HVDC (High Voltage Direct Current) bus that feeds the high power loads such as flight controls surfaces (FC), de ice or emergency braking for a maximum consumption estimated to 27 kW. These essential loads have to be powered during emergency cases. We also have to face with 5 kW of “rejected power” as with certain actuators that could be bidirectional (FC in closure operation for instance).
- A 28 V LVDC (Low Voltage Direct Current) bus supplying “avionic bus” with flight computers estimated as a constant power load of 4 kW. While the RAT is assumed to be connected to the HVDC bus, the storage device is connected between those two buses at a “Medium Voltage”. As shown on the right part of Fig. 1, a particular solution could also be considered with the accumulators directly plugged on the LVDC 28 V bus as on classical aircrafts. Thus, it becomes necessary to study and size the power converter units that have to be implemented depending on the chosen “Medium Voltage”.

In any case, a galvanic insulation should be provided in the MVDC/LVDC or HVDC/LVDC power converter in order to avoid perturbation on the LVDC bus induced by a failure on the power loads.

In order to set the context of this study and application, the authors firstly present the experimental validation of the hybridization concept with a low voltage lithium ion battery (28 V) on a test bench. This battery was already tested in the laboratory and this one is used on the LVDC bus electrical network aircraft to supply the flight computers: it corresponds to the particular solution presented on the right part of Fig. 1. Afterward, the work presented in this paper mainly aims at estimating the best connection voltage of the accumulators in terms of mass and efficiency for the embedded power electronics. It also takes into account the mass of the considered storage device advised by the manufacturer. The paper mainly refers to the models used to design the components that are connected in the power converter units. Some first results are presented to establish the optimal connection voltage.

2. Experiments on a hybrid emergency network: particular case of a 28 V accumulator

2.1. Hybridization control strategies

There are two basic strategies for hybridization of generator with a lithium ion battery, both having individual advantages and drawbacks. A Low Pass Filtering (LPF) of the load current is done in both strategy cases in order to set the power sharing between each source. The filtering frequency of the LPF has to be chosen to optimize the system

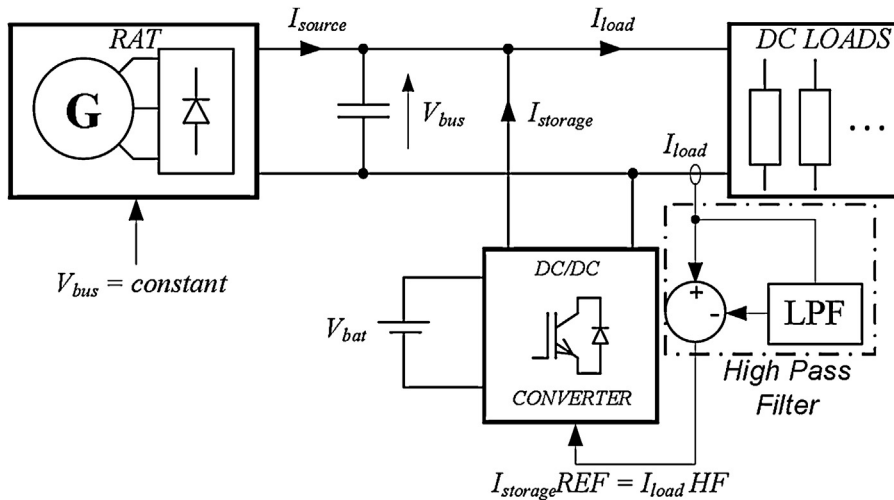


Fig. 2. Schemes of hybridization control structures with battery in current mode.

management and the storage sizing. This choice is depending on the characteristics of the load power profile. More details on these strategies are provided in [14].

The excitation field circuit is used to fulfill its control objective for all the RAT operation modes (voltage, current, or MPPT mode).

The first strategy, with battery in “current mode” (Fig. 2), operates the RAT as a constant voltage source and the storage bank as a transient current source (I_{source}). The reference current for storage is the high frequency component of the load current ($I_{load HF}$) obtained from the low pass filtering: $I_{load HF} = I_{load} - LPF(I_{load})$. Consequently, the RAT only provides the average power and low frequencies of the load power by only keeping constant the DC voltage bus. Due to the high pass filtering effect, the storage subsystem only provides the intermittent power, especially due to flight control surface motion, with harmonics beyond the filter cut off frequency.

In the second strategy with battery in “voltage mode” (Fig. 3), the source natures are swapped: the RAT is used as a current source, while the storage system is responsible for controlling the DC bus voltage. In this case, the reference current of the RAT is the low pass filtered load current ($I_{RAT REF} = LPF(I_{load})$). As for classical wind turbine systems,

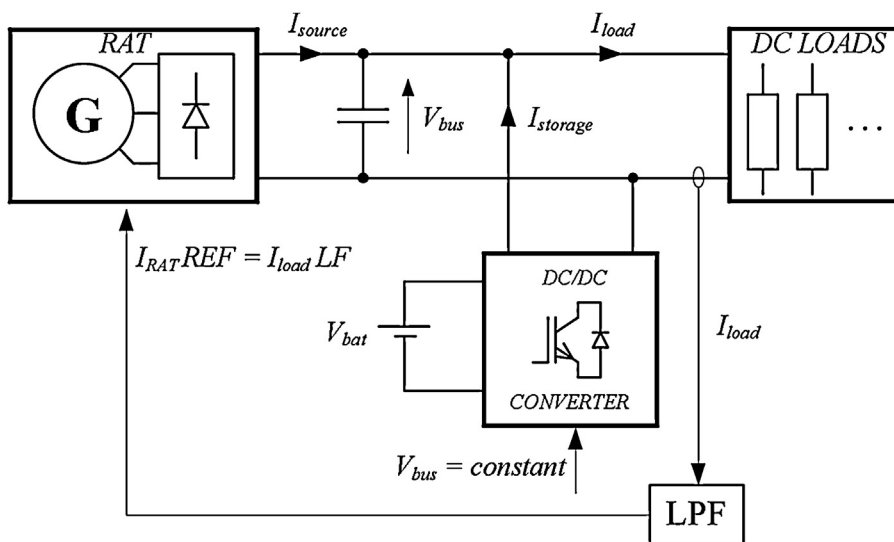


Fig. 3. Schemes of hybridization control structures with battery in voltage mode.

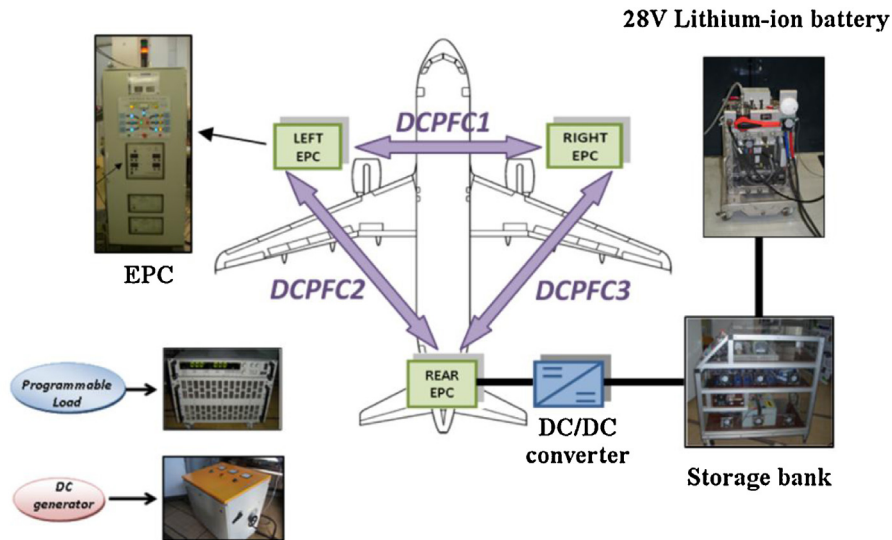


Fig. 4. Structure of the electrical network.

when the power demand is high, this strategy allows maximizing the RAT power with an MPPT (Maximum Power Point Tracking) mode.

Optimizing the energy transfer leads to minimize the RAT sizing and consequently the whole system weight [14]. The average power consumption of the load and system losses are supplied by the RAT while intermittent powers are fed by the lithium ion battery.

In Figs. 2 and 3, the DC/DC power converter allows:

- interfacing a HVDC bus with a low voltage battery,
- controlling the current $I_{storage}$ when the storage bank operates in current mode.

2.2. Experimental laboratory test bench

The LAPLACE laboratory is equipped with an experimental test bench which reproduces the electrical system of a future more electrical aircraft (Fig. 4).

The hearts of the system are three EPC's (electrical power centers). Each of them is able to interconnect up to six DC sources and loads with a maximum current of 50 A. Power exchange between each EPC is possible with DCPFC's (Direct Current Power Flow Controllers) [2]. DCPFCs are static converters, which can be controlled in voltage mode or current mode. As the LAPLACE laboratory is not equipped with an actual RAT, this latter has been emulated by DC generators constituted of three phase autotransformers with diode rectifiers. The lithium ion battery is connected to the storage bank. The overview of the experimental bench is presented in Fig. 5.

The control of energy management strategies has been programmed via Matlab/Simulink. The whole system (DCPFC, DC/DC converter, contactors placed in EPC's) is managed by a DSPACE supervisor and the ControlDesk software. A special ControlDesk layout has been created for the hybridization control. In this layout, the choice of the hybridization strategy is selected. According to the strategy chosen, the DSPACE manages the experimental bench and emulates the emergency mission. The power converters used in the presented experiment allow operating at 10 kW peak power.

2.3. Experimental results

This section presents some results, obtained in the LAPLACE laboratory, with the electrical emergency network. Several mission profiles, corresponding with typical flight cycles in case of TEFO (Total Engine Failure Operation), have been applied for the hybridization of the RAT with the lithium ion battery. Two main generator failures have been

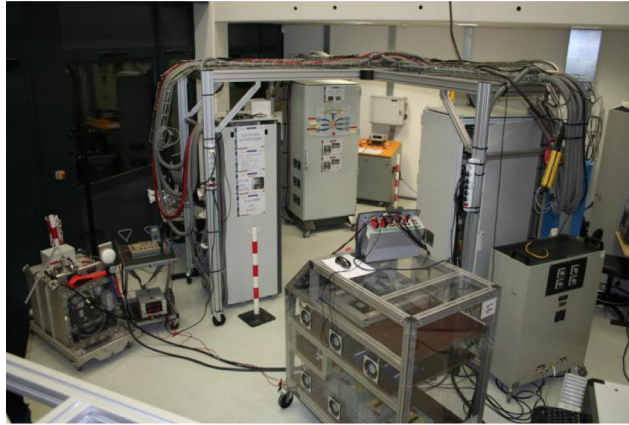


Fig. 5. The experimental test bench.

implemented in the experimental test bench: on the one hand, the voltage drops of main generator at 10% below the voltage reference, on the other hand, the lost of the connection between the main generators and the HVDC bus. When the failure is detected, the emergency mode is immediately activated, the main generator is isolated (power contactor opening) from the HVDC bus. Then, the storage device, through the DC/DC converter, allows maintaining the HVDC bus. The configuration of the experimental test bench is represented in Fig. 6. A DC generator (GEN) connected at the right EPC combined with the DCPFC3 emulates the main generator. The other GEN connected at the left EPC and the DCPFC2 emulates the RAT during the emergency mission. A bidirectional DC/DC converter allows connecting the lithium ion battery with the HVDC bus. The voltage level of the HVDC bus is chosen at 270 V. This HVDC bus voltage allows obtaining stable performance of the dynamic loads connected at the rear EPC which emulate the profile of the emergency mission.

Among a set of tested strategy, we illustrate in this section one particular energy management strategy which has been implemented on the dSPACE supervisor (Fig. 7): the chosen strategy is the one illustrated in Fig. 3.

In “normal operating mode”, the main generator is connected to the HVDC bus.

When a failure is detected (“Gen failure”) on the main generator (the voltage of the main generator drops), the emergency mode is activated. A power contactor disconnects the main generator to the HVDC bus. During the “RAT deployment”, the battery is the only source to provide energy in the aircraft network. After the failure detection, the power converter connected to the storage device is switched on to maintain the voltage of the HVDC bus: during this critical period, a pre-load circuit with transient resistors should be switched on if the HVDC bus voltage is too low. Note that, with the hybrid structure, this transition is shorter than in the case with a RAT alone, the RAT deployment

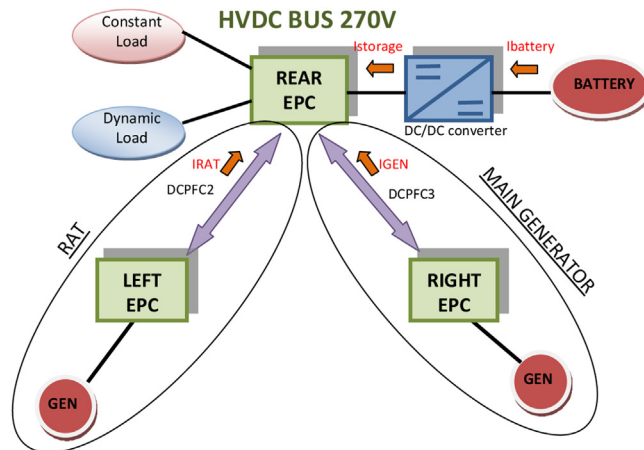


Fig. 6. Configuration of the test bench.

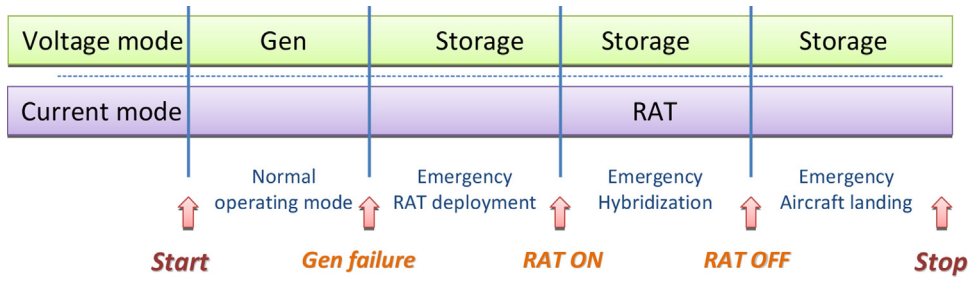


Fig. 7. Management strategy of the emergency mission, with storage in voltage source.

taking some seconds. A “no break power operation” can then be ensured by controlling the HVDC bus with the battery as illustrated in Fig. 7. For that purpose, the capacitor of the HVDC bus is sized to limit the voltage drop on the bus during this commutation mode.

When the RAT is available, the hybridization is normally operating and the RAT is controlled in current mode as in the strategy of Fig. 3. When the aircraft is landing, the airspeed of the RAT is not sufficient to produce the power, and the battery is one more time the only source in the network. Note that this strategy minimizes the number of control algorithm switching, the HVDC bus being always controlled from the storage device from the failure detection till the end of mission.

The mission profile is emulated as illustrated in Fig. 8. The target of this mission profile is to check the feasibility of the hybridization on the experimental test bench. Hence, the power level of this profile is lower than the power level in the actual emergency network. In normal operating mode and hybridization mode, the load power is fluctuant while the load power is constant when the battery is alone.

In Fig. 9, experimental results obtained on the lab test bench are presented, with the system being configured as follows:

- Lithium ion battery, nominal voltage; 28 V, capacity: 60 Ah
- HVDC bus voltage is controlled to 270 V
- The cut off frequency of the low pass filter is set at 10 mHz regarding this mission profile and the battery sizing.

During this strategy management, the RAT provides only the low frequency part of load current (the current of the RAT is nearly constant). The DC/DC converter, which is connected to the battery, provides the high frequency harmonics. However, the frequency bandwidth of the DC/DC converter, placed in our lab test bench, is too low to provide the totality of high frequency components. Then, the other high frequencies, which are not supported by the DC/DC converter, are provided by the bus capacitors which impact the regulation of the bus voltage. A DC/DC converter with a better bandwidth would lead to better control the HVDC bus voltage during the hybridization.

These experimental results have shown the feasibility of the hybridization principle with a RAT and a lithium ion battery. Two significant advantages lead to choose the RAT in current mode control with storage in HVDC bus regulation:

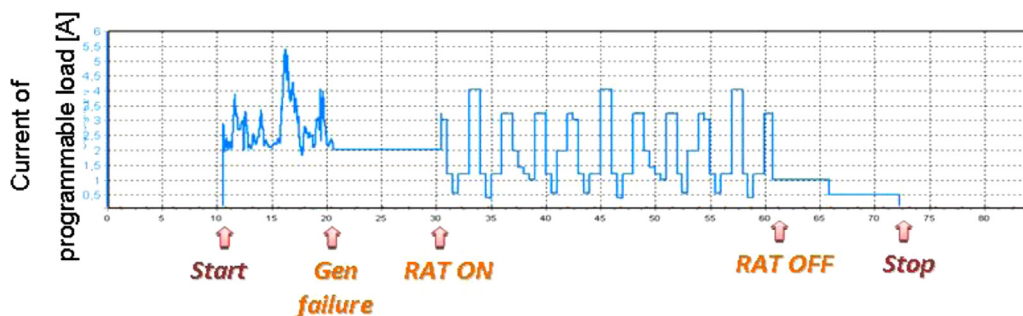


Fig. 8. Power mission profile emulated from a programmable load.

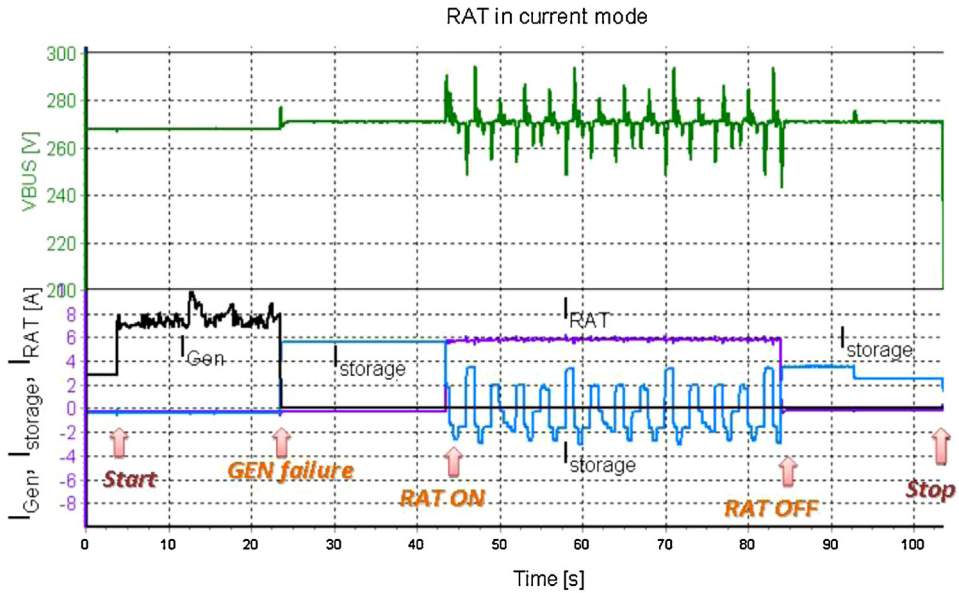


Fig. 9. Hybridization tests with RAT emulation.

1. This strategy offers the possibility to implement a Maximum Power Point Tracking algorithm to exploit RAT in optimal conditions as for classical wind turbines [14].
2. As illustrated in Fig. 7, the storage device is continuously in voltage mode from the TEFO state, which minimize the number of algorithm switching (switching between voltage/current mode), contrarily to the strategy case for which the RAT control the HVDC voltage during the hybridization phase.

The following of this paper aims at estimating the best connection voltage of the accumulators in terms of mass and efficiency for the embedded power electronics.

3. Power converter topologies

3.1. 'Noninsulated' buck boost topology

The first topology used to ensure the MVDC/HVDC conversion is equivalent to a classical bidirectional Boost converter with IGBT/Diode modules (Fig. 10). It is here sized for 27 kW in boost mode and 9 kW in buck mode. We also take into account the possibility to interleave several branches or switches in parallel. It allows us to estimate weight and losses on a wide range of structures and sizing that fulfil the requirements for different connection voltages on the MVDC bus.

Electrical values such as current ripple, rms or average currents in switches, inductance, capacitance, etc. are calculated using basic equations referring to classical Boost converter [7].

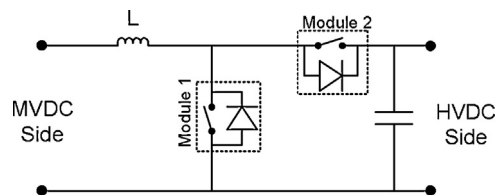


Fig. 10. Noninsulated topology.

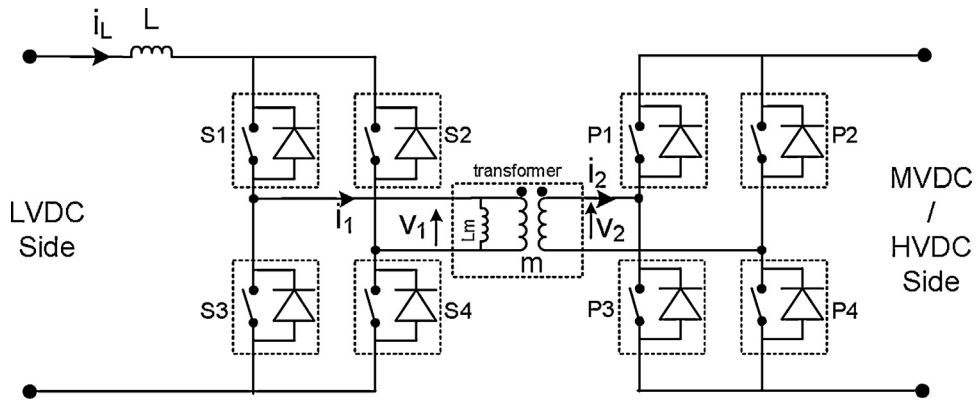


Fig. 11. Insulated topology.

3.2. 'Insulated' buck boost topology

The second topology is a dual H bridge insulated bidirectional DC/DC converter with MOS/Diode modules on the low voltage bridge and IGBT/Diode on the medium voltage side (Fig. 11). It is considered as a solution for the MVDC/LVDC conversion as well as the LVDC/HVDC conversion in the case of accumulators connected on the LVDC bus.

In Fig. 11, the current of the inductor is noted i_L , i_1 and v_1 are respectively the current and the voltage on the primary side of the transformer. On the secondary side, they are noted i_2 and v_2 . The turn ratio and the magnetizing inductor of

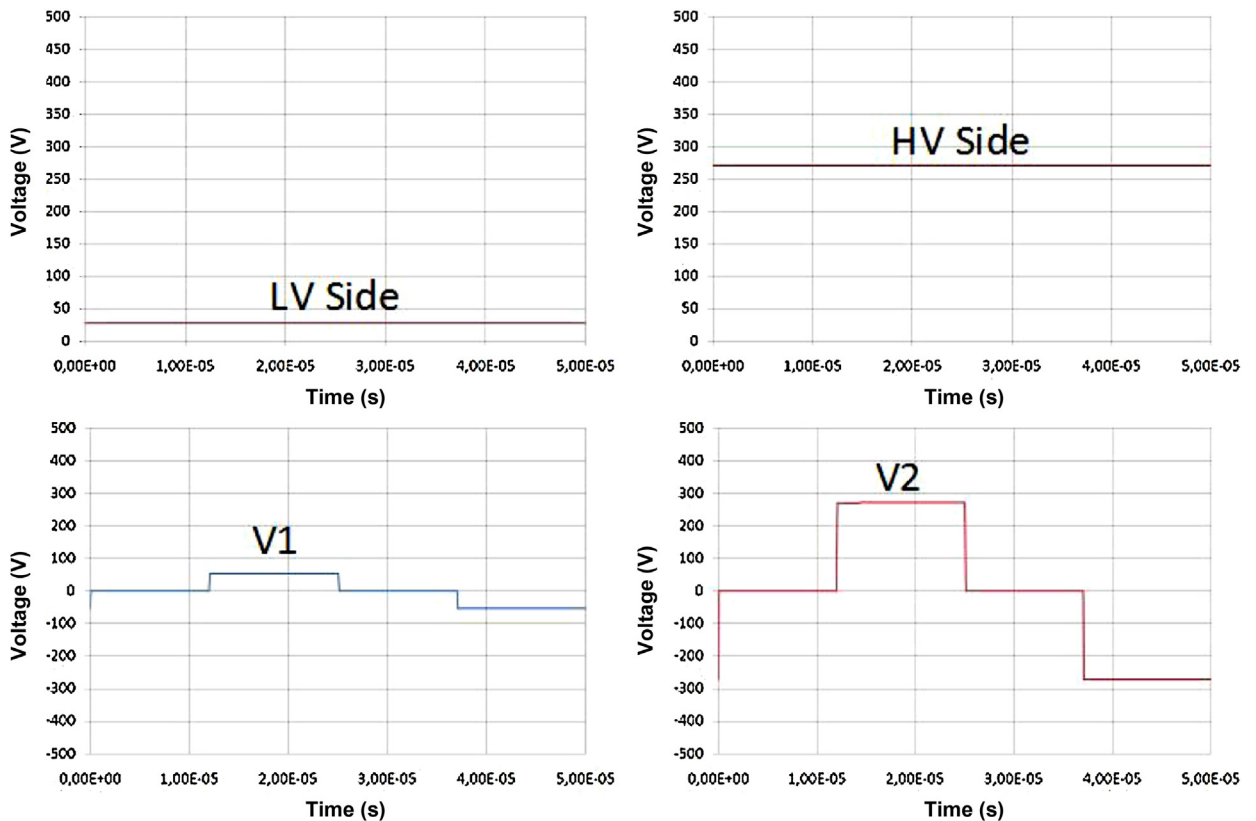


Fig. 12. Voltage waveforms.

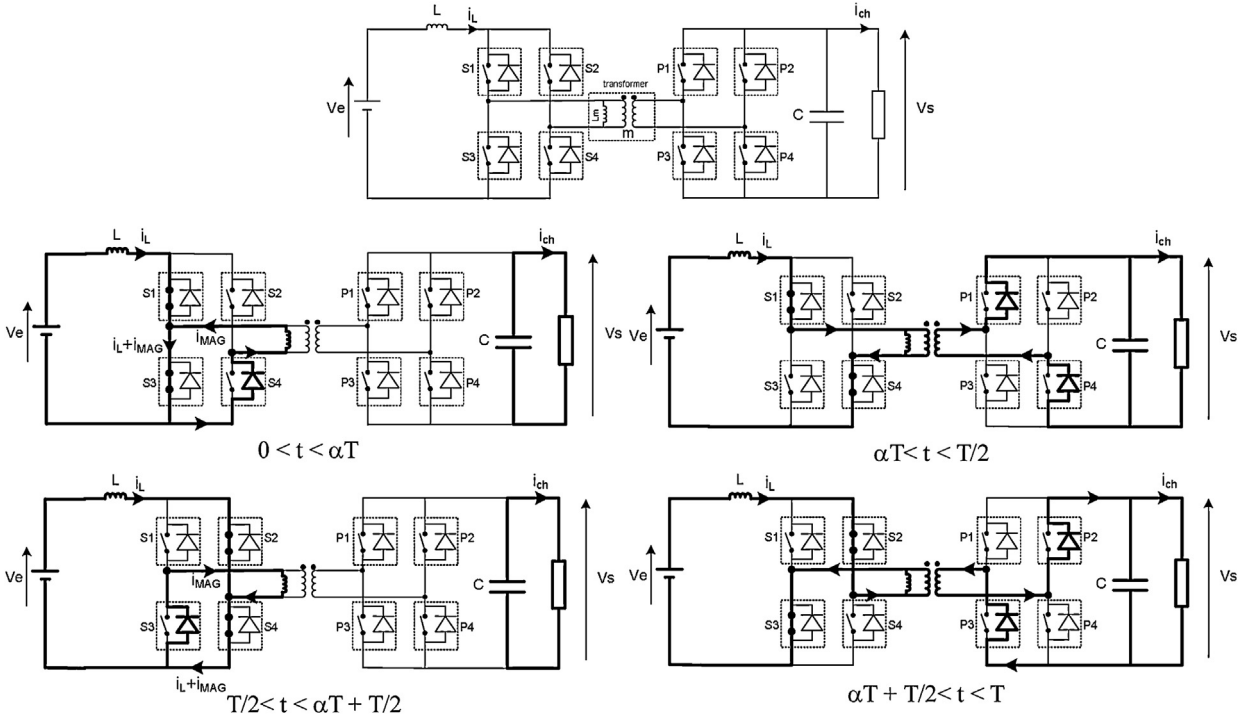


Fig. 13. Isolated Buck Boost converter in Boost mode.

the transformer are respectively called m and L_m . To reduce the overvoltage spikes during commutations of the power switches, a snubber circuit (a resistor in series with a capacitor) could be placed [17]. For the dimensioning of this power converter, the impact of the snubber circuit on the efficiency and the mass have not been implemented in the design strategy.

The time operation of the voltage transformation from input to output stage can be summarized in Fig. 12 with a low voltage of 28 V and a medium voltage of 270 V.

3.2.1. Boost mode

In boost mode, only the switches on the low voltage side are controlled while the other bridge could be assimilated to a diode rectifier. Fig. 13 presents the topology of the isolated Buck Boost converter in Boost mode and the operation modes on the period of the switching frequency noted T . The switching signals in Boost mode are shown in Fig. 14.

In that case, V_e and V_s are the LVDC and HVDC voltages. I_e is the DC component of i_L . We also use P as the sizing power, I_{MAG} being the estimated magnetizing current, f_{dec} the switching frequency and α the duty cycle. Assuming continuous conduction mode, we calculate:

- Transfer function:

$$\frac{V_s}{V_e} = \frac{m}{(1 - 2\alpha)}$$

- Inductance:

$$L = \frac{\alpha V_e}{\Delta I L \times f_{dec}} \quad \text{calculated for a duty cycle equal to 1.}$$

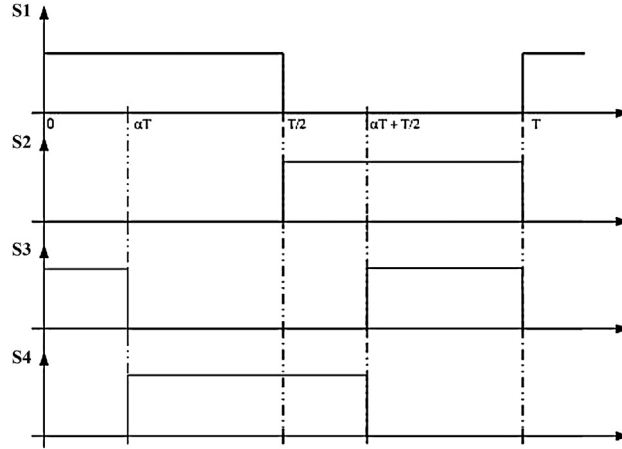


Fig. 14. Switching signals in Boost mode.

$$IL_{\max} = I_e + \frac{\Delta IL}{2} = \frac{P}{V_e} + \frac{\Delta IL}{2} \quad \text{and} \quad IL_{RMS} = \sqrt{I_e^2 + \frac{\Delta IL^2}{12}}$$

- Capacitor:

$$C = \frac{(1 - 2\alpha)(\Delta IL + \Delta I_{MAG})}{\Delta V_s \times m \times f_{dec}}$$

$$I_{C_{RMS}} = \sqrt{(1 - 2\alpha)I_{ch}^2 + 2\alpha I_{c_{\max}}^2 - \frac{2\alpha}{m} I_{c_{\max}} \Delta IL + \frac{2\alpha}{3m^2} \Delta IL^2}$$

- Switches (with I_{MAG} equal to zero):

$$I_{S_{moy}} = \frac{IL_{moy}}{2} = \frac{I_e}{2} \quad \text{and} \quad I_{S_{RMS}} = \frac{IL_{RMS}}{\sqrt{2}}$$

$$I_{p_{moy}} = \frac{((1/2) - \alpha)I_e}{m} \quad \text{and} \quad I_{p_{RMS}} = \frac{1}{m} \sqrt{I_e^2 \left(\frac{1}{2} - \alpha\right) + \Delta IL^2 \left(\frac{1 - 2\alpha}{24}\right)}$$

- Transformer:

$$I_{l_{RMS}} = \sqrt{(1 - 2\alpha)I_e^2 + \Delta IL^2 \left(\frac{7 - 14\alpha}{6}\right) + 2\alpha I_{MAG}^2}$$

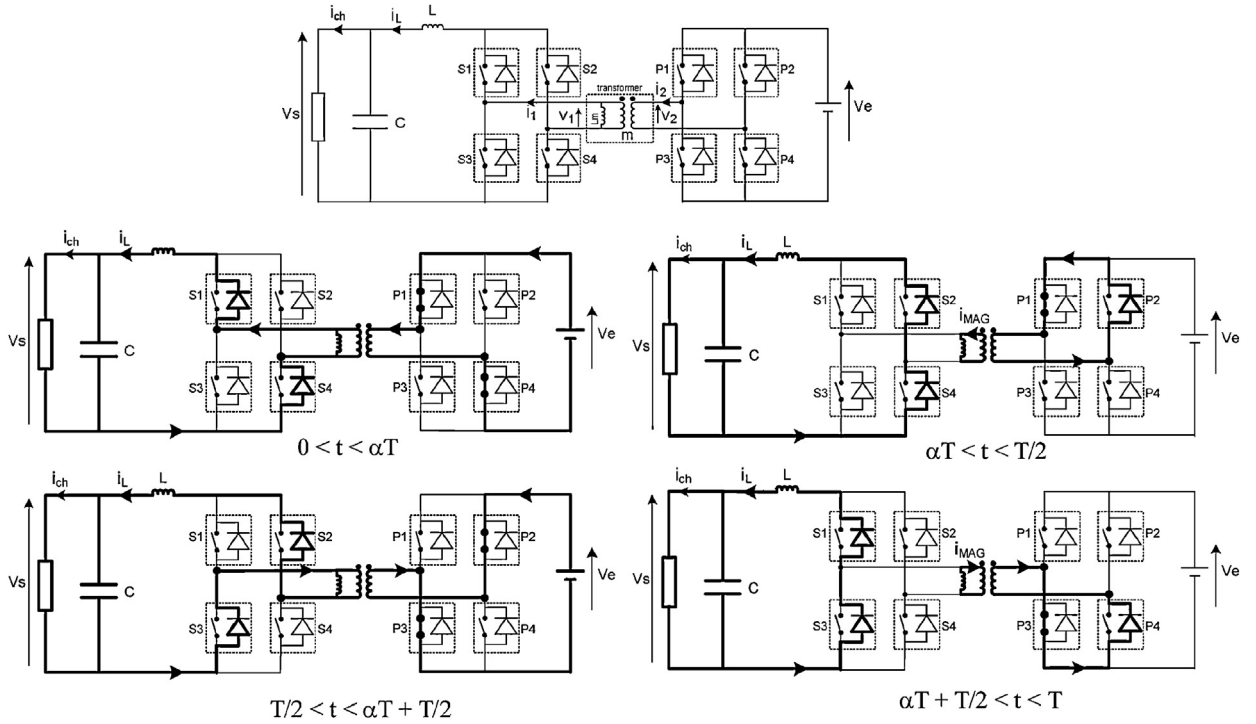


Fig. 15. Isolated Buck Boost converter in Buck mode.

$$I_{2RMS} = \frac{\sqrt{2}}{m} \sqrt{I_e^2 \left(\frac{1}{2} - \alpha \right) + \Delta I L^2 \left(\frac{1 - 2\alpha}{24} \right) + \Delta I_{MAG}^2 \left(\frac{1 - 2\alpha}{24} \right) + \Delta I_{MAG} \Delta I L \left(\frac{5 - 10\alpha}{24} \right)}$$

3.2.2. Buck mode

The topology of the power converter in Buck mode and all the operation modes are indicated in Fig. 15.

The switching signals in Buck mode are shown in Fig. 16.

Electrical values for the embedded components are calculated just like previously in a continuous conduction mode. In that case the input voltage V_e is the HVDC while V_s is the MVDC or LVDC if the accumulators are directly connected at 28 V. I_s is the DC component of i_L .

- Transfer function:

$$\frac{V_s}{V_e} = \frac{2\alpha}{m}$$

- Inductance:

$$L = \frac{(0.5 - \alpha)V_e}{\Delta I L \times f_{dec}}$$

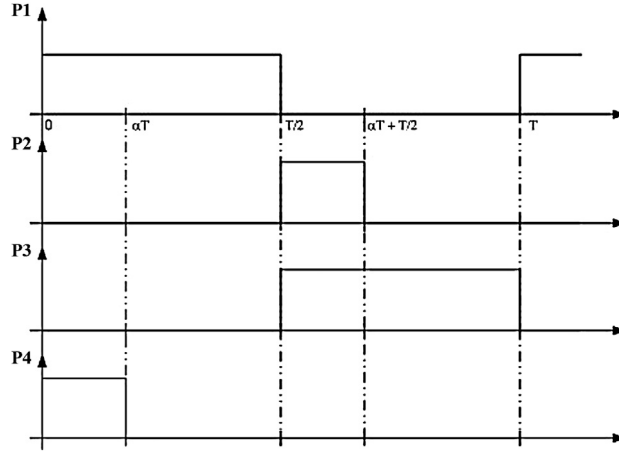


Fig. 16. Switching signals in Buck mode.

$$IL_{\max} = I_s + \frac{\Delta IL}{2} = \frac{P}{V_s} + \frac{\Delta IL}{2} \quad \text{and} \quad IL_{RMS} = \sqrt{I_s^2 + \frac{\Delta IL^2}{12}}$$

- Capacitor:

$$C = \frac{\Delta IL}{8\Delta V_s f} \quad \text{and} \quad I_{CRMS} = \sqrt{\frac{\Delta IL^2}{12}}$$

- Switches ($I_{MAG} = 0$):

$$I_{Smoy} = \frac{IL_{moy}}{2} = \frac{I_s}{2} \quad \text{and} \quad I_{SRMS} = \frac{IL_{RMS}}{\sqrt{2}}$$

$$I_{pmoy} = \frac{\alpha I_s}{m} \quad \text{and} \quad I_{pRMS} = \frac{1}{m} \sqrt{\alpha I_s + \alpha \frac{\Delta IL^2}{12}}$$

- Transformer:

$$I_{lRMS} = \frac{\sqrt{2}}{m} \sqrt{\alpha I_{ch}^2 + \alpha \frac{\Delta IL^2}{12} + \alpha \frac{\Delta I_{MAG}^2}{12} + \alpha \frac{\Delta I_{MAG} \Delta IL}{6} + \frac{\Delta I_{MAG}^2}{8} (1 - 2\alpha)}$$

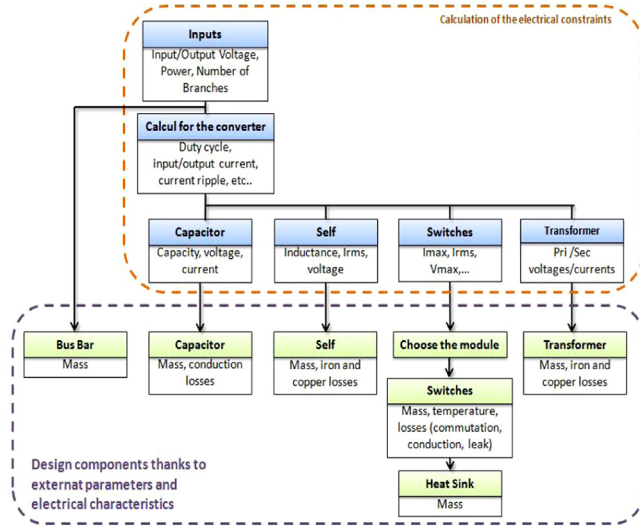


Fig. 17. Design strategy.

$$I2_{RMS} = \sqrt{2\alpha I ch^2 + \frac{7\Delta IL^2}{6}}$$

For both boost and buck mode we have to take into consideration the number of interleaved branches as well as the number of switches connected in parallel. The duty cycle is calculated with the input/output voltage. If it is below 0.5 the previous formulas remains applicable. On the contrary, if the calculated duty cycle α over 0.5, the formula is used and we replace $\alpha' = 0.5 - \alpha$.

3.3. Design strategy

The mass and efficiency of the embedded power converter will depend on the voltage connection of the accumulators. In order to appreciate the best solution, power electronics corresponding to various solutions have to be sized. Once the MVDC voltage is entered and the numbers of interleaved branches and switches are defined, we calculate electrical characteristics using the above formulas implemented in spreadsheets. The spreadsheets allow calculating the characteristics of the components in order to respect the input data specifications. The design strategy is presented in Fig. 17.

The mass and efficiency of the whole converter are estimated from the design of the components [8]:

$$W_{Convert} = 1,35 \times \sum W_{Components} \quad \eta_{CVS} = \frac{P - \sum losses}{P}$$

4. Models used to design the devices

4.1. Capacitors

Weight (W_c) and internal resistance (R_c) of capacitors are calculated with the maximum voltage and the desired capacity using formulas established from datasheets:

$$W_c = 4.36.10e^{-2} \times V + 214.17 \times C^{0.124}$$

$$R_c = 4.29.10e^{-4} \times V + 0.66 \times C^{0.073}$$

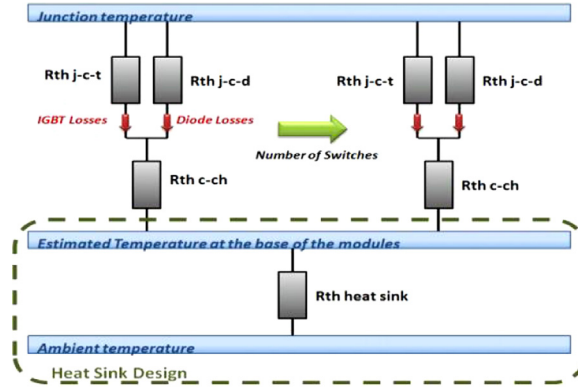


Fig. 18. Thermal model for IGBT/diode modules.

4.2. Bus bar

The weight of the bus bar is given by the following formula [8]:

$$W_{bb} = \frac{1.33}{6} \times nb_{//Branches} \times nb_{//Switches}$$

4.3. Switches

Switching, conduction and leakage losses for both IGBT/Diode modules and MOS/Diode modules are calculated like in [8] taking into account the ratio between test conditions and electrical values calculated in our application. For instance, the following formula is used to estimate the IGBT switching losses:

$$PSwitch_{IGBT} = (E_{on}(I_{IGBT}) + E_{off}(I_{IGBT})) \times f \times \frac{V_{IGBT}}{V_{Test}}$$

In the same time, we get an idea of the mass of the embedded silicon and the temperature at the base of the components is determined with the calculated losses and the following model (Fig. 18).

4.4. Heat sink

We consider a forced convection cooling system and a dissipator with winglets (Fig. 19) in order to ensure an operating temperature below the maximum junction temperature.

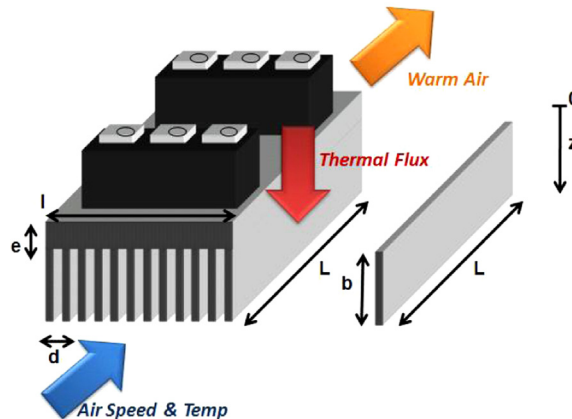


Fig. 19. Considered heat sink.

We consider heat transfer problems and especially the Newton's law giving the thermal energy exchanged between the ambient pulsed air and the heat sink with h the heat transfer coefficient (W/m^2) and S the heat exchange area:

$$\Phi = hS(T_{\text{HeatSink}}(z) - T_{\text{Air}})$$

where

$$T_{\text{HeatSink}}(z) = \frac{T_{\text{Air}} - T_{\text{Module}}}{b}z + T_{\text{Module}}.$$

The thermal energy that could be dissipated by the designed heat sink in operating conditions will be mainly estimated through the value of the heat transfer coefficient h . That value is taken from a dimensionless number called the Nusselt number (Nu). It is extrapolated using the Colburn correlation for a turbulent flow, with the Reynolds (Re) and Prandtl (Pr) numbers that define the characteristics of the flow at a given temperature and speed [3]. With λ the conductivity of the fluid:

$$\overline{Nu} = 0.023Re^{0.8}Pr^{0.33} \quad \text{and} \quad Nu = \frac{hd}{\lambda}$$

Once the Nusselt number is known, we calculate the total heat energy dissipated with the following formula where nb_{wing} is the number of winglets:

$$\Phi = hL(b + d)(T_{\text{Module}} - T_{\text{Amb}})(nb_{\text{Wing}} - 1)$$

The design of the component is optimized in terms of mass checking that all losses are dissipated and that the flow remains turbulent (Re over 10,000).

4.5. Inductors

The chosen cores for inductors are U cores in ferrite (3C90) with flat conductors. The air gap e is distributed in the structure as shown in Fig. 20. With the geometry of the circuit, we calculate the magnetic reluctance with a permeability depending on a magnetic field define as B_{calc} . Hence, we access to the true magnetic field with the operating conditions. Once the alternative component of the magnetic field is known, iron losses are estimated using the Steinmetz formula where T_{calc} is the supposed temperature of the component [5,18]:

$$dP_{\text{fer}} = Cm \times f^x \times \left(\frac{B_{AC}}{2}\right)^y \times (ct0 - ct1T_{\text{calc}} + ct2T_{\text{calc}}^2)$$

$$dP_{\text{fer}} = Cm \times f^x \times \left(\frac{B_{AC}}{2}\right)^y \times (ct0 - ct1T_{\text{calc}} + ct2T_{\text{calc}}^2)$$

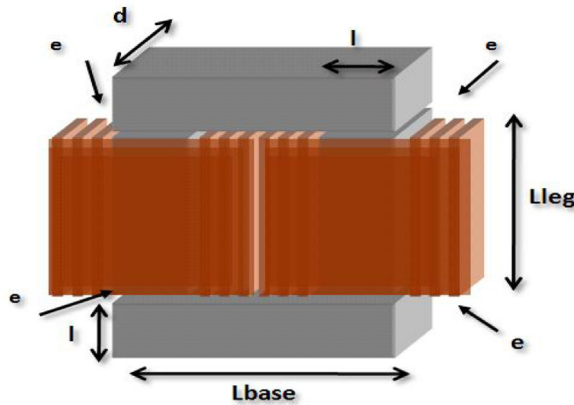


Fig. 20. Considered inductor.

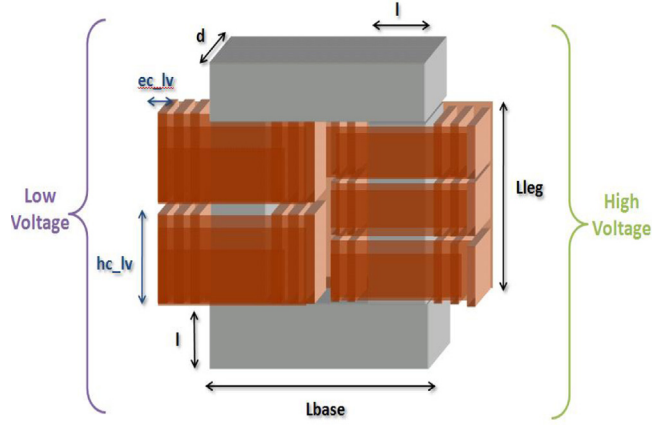


Fig. 21. Considered transformer.

The direct resistance of the conductors is calculated with a resistivity ρ depending on the operating temperature T_{calc} , Nt being the number of turns, with the thickness of both conductors (ec) and insulation (dc)

$$R_{DC} = \frac{\rho \times (Nt(d + l + 2dc) + ((Nt - 1)Nt)/2(ec + dc))}{L_{leg} \times ec}$$

The alternative resistance is with the Dowell's model given for transformer winding with the skin depth δ [6]:

$$F_R = \frac{R_{AC}}{R_{DC}} = X \underbrace{\frac{\sinh 2X + \sin 2X}{\cosh 2X - \cos 2X}}_{\text{Skin Effect}} + 2X \underbrace{\frac{m^2 - 1}{3} \frac{\sinh X - \sin X}{\cosh X + \cos X}}_{\text{Proximity Effect}}$$

where $X = ec/\delta$ and m is the number of layers in the winding.

Then the heating of the component is calculated with the Newton's law where $h = 5 \text{ W/m}^2 \text{ K}$ that corresponds to average natural convection according to [3]. The heat transfer area S is assumed to be the overall surface of the sized component.

$$T_{Induc} = T_{Amb} + \frac{1}{hS} \times Losses$$

The design is optimized in term of mass and we pay attention to the difference between T_{calc} and T_{Induc} and between B_{calc} and B_{Induc} that have to be below 5%. In addition, many constraints have to be respected such as overheating, saturation of the ferromagnetic material, current density, area product.

4.6. Transformers

The sizing strategy for transformers is very similar to the previous one presented for inductors (Fig. 21).

One main difference is noticed for the copper losses. For each winding, we calculate the number of layers depending on the number of turns Nt and the geometry.

$$Nb_{layers} = ENT \left(\frac{Nt}{ENT((L_{leg}/hc) + 1)} + 1 \right)$$

$$R_{DC} = \frac{\rho \times (Nt(d + l + 2dc) + ((Nb_{layers} - 1)Nb_{layers})/2)(ec + dc) \times ENT((L_{leg}/hc) + 1)}{hc \times ec}$$

The same constraints have to be respected in the case of the transformers. In addition, we have to control the turn ratio as well as the value of the magnetizing current below 5% of the current flowing in windings on the low voltage side.

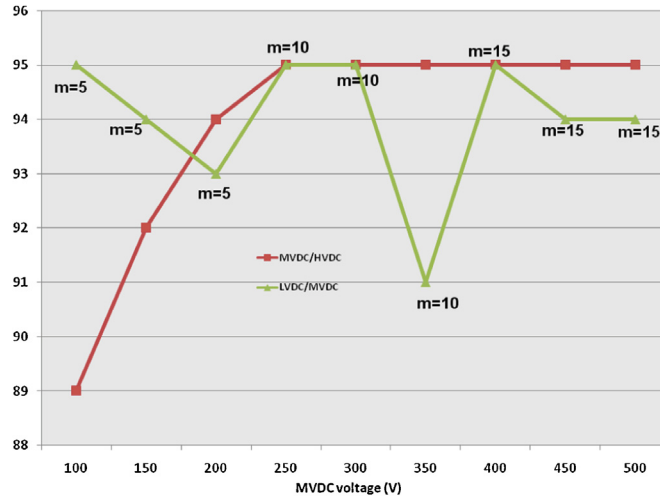


Fig. 22. Efficiency of power converters (%).

5. Results of sizing

All the previous models have been implemented in the same tool in order to estimate the weight of power electronics corresponding to different connection voltages of the storage device. The design has been processed with a switching frequency at 20 kHz, an ambient temperature at 50 °C, a maximal junction temperature of switches at 125 °C, a maximal temperature of magnetic cores at 150 °C and an air speed in the heat sink at 10 m/s. Some hypotheses also remain the same whatever the considered solution. The maximum voltage ripple is fixed at 1% while the current ripple should not exceed 10%.

5.1. LVDC accumulator

For this network configuration (right part of Fig. 1), a LVDC (28 V)/HVDC (540 V) isolated buck boost power converter (BBCU) is used. The design strategy has allowed obtaining a mass of 34 kg and 80% for efficiency. The mass of the 28 V battery is estimated at 48 kg.

5.2. MVDC accumulator

Both insulated and noninsulated converters are needed for this strategy of connection (left part of Fig. 1). Fig. 22 refers to the evolution of efficiencies for both power converters according to the MVDC voltage. Increasing the MVDC voltage is better for the efficiency of the noninsulated topology that ensures the MVDC/HVDC conversion (reduced power losses in power switches). For the insulated buck converter, the turns ratio of the transformer m has a major impact and we notice that losses in the switches and in the transformer are the most significant.

The mass of the insulated power converter increases with the MVDC voltage whereas it is the opposite for the buck/boost converter (Fig. 23). For both insulated and noninsulated topologies most of the mass is caused by the magnetic components. Thus it could be interesting to study the sensitivity of the model versus parameters such as heat transfer coefficient or saturation of the magnetic material but it is not discussed in the present paper.

5.3. Mass of the system

Fig. 24 presents the mass of the system versus the connection voltage. At high connection voltages the mass of the accumulator increases with the voltage because there are more cells in series whereas at low levels we have to connect several branches in parallel to ensure the mission in term of energy which also led to a mass increase. Finally the optimum for the connection voltage appears to be between 200 V and 300 V.

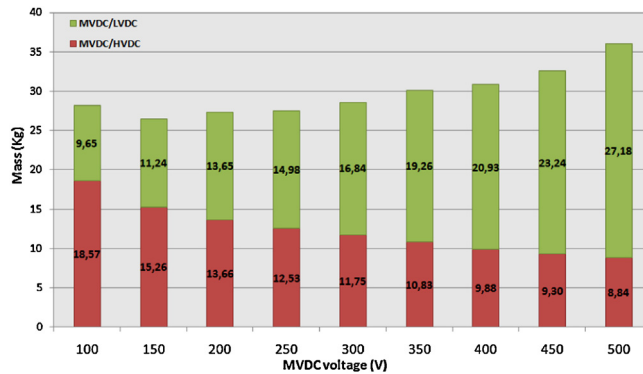


Fig. 23. Mass of the power converters.

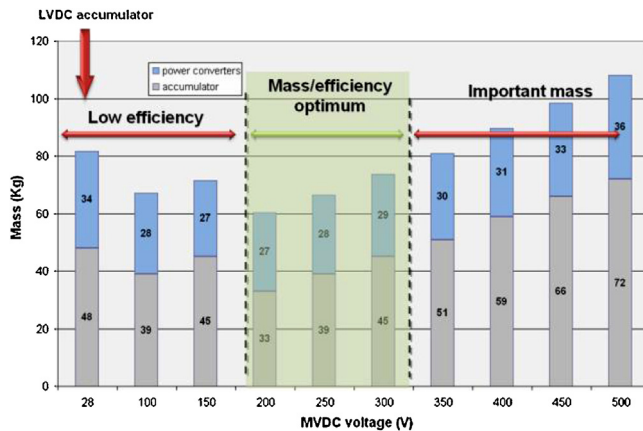


Fig. 24. Mass of the overall system.

6. Conclusion

In this paper, one hybridization strategy has been tested on an experimental test bench that interfaces an emulator of RAT device and a 28 V lithium ion battery subsystem interfaced with a DC/DC bidirectional converter. The converter structure allows interfacing a HVDC bus with low or even very low storage voltages. The main generator (RAT subsystem) and the load are connected to a HVDC bus, they physically emulate actual dynamics of the aircraft emergency electrical network. In the second part of this paper, we have developed basic models for the components of power converter units. Using simple hypotheses, we have processed a pre sizing in terms of mass and efficiency that has proved to be valuable to determine the best connection voltage of the storage device. The design strategy is optimized for the heat sink and magnetic components. In a further development, we could process a multiobjective optimization to find for each voltage the appropriate number of interleaved branches or switches, and the best turn ratio. Several future experimental tests will be carried out on the lab test bench with a medium-voltage lithium ion battery (224 V).

Acknowledgments

This study has been involved in the framework of the ISS (Innovative Solution for Systems) national project for which the authors thank the DGAC (Direction Générale de l'Aviation Civile) and Airbus operation SAS for support and funding. Authors also like to thank SAFT for scientific cooperation.

References

- [1] ACARE, Advisory Council for Aeronautics Research in Europe, Aeronautics and air transport, ACARE success stories, issue March, 2011. Available from: URL: http://www.acare4europe.org/docs/ACARE_Success_Stories_Final.pdf.

- [2] C. Baumann, H. Piquet, X. Roboam, E. Bru, A mixed function for actuation and power flow control in embedded networks, *IEEE Transactions on Industrial Electronics* 59 (9) (2012) 3596–3603 (special issue More Electrical Aircraft).
- [3] A. Bejan, A.D. Krauss, *Heat Transfer Handbook*, John Wiley & Sons Inc., Hoboken, NJ, 2003.
- [4] I. Christou, A. Nelms, I. Cotton, M. Husband, Choice of optimal voltage for more electric aircraft wiring systems, *IET Electrical Systems in Transportation* 1 (1) (2011) 24–30.
- [5] Design of Planar Power Transformers, Application Note, Ferroxcube, 1997.
- [6] P.L. Dowell, Effects of eddy currents in transformer windings, *Proceedings of IEE* 133 (8) (1966) 1387–1394.
- [7] R.W. Erickson, D. Maksimovic, *Fundamental of Power Electronics*, second ed., Springer, 2001.
- [8] M. Garcia Arregui, Theoretical study of a power generation unit based on the hybridization of a fuel cell stack and ultracapacitors, Ph.D. Thesis, Institute National Polytechnique, Toulouse, 2007. Available from: URL: <http://ethesis.inp-toulouse.fr/archive/00000521/>.
- [9] D. Izquierdo, R. Azcona, F.J. López del Cerro, C. Fernández, B. Delicado, Electrical power distribution system (HV270DC) for application in more electric aircraft, in: *APEC, Twenty Fifth Annual IEEE*, 2010, pp. 1300–1305.
- [10] O. Langlois, Conception d'un réseau de secours électrique pour l'aéronautique, Ph.D. Thesis, Institut National Polytechnique, Toulouse, 2006. Available from: URL: <http://ethesis.inp-toulouse.fr/archive/00000243/>.
- [11] A. Lücken, J. Brombach, D. Schulz, Design and protection of a high voltage DC onboard grid with integrated fuel cell system on more electric aircraft, in: *ESARS Conference*, 2010, pp. 1–6.
- [12] K. Rafal, B. Morin, X. Roboam, E. Bru, C. Turpin, H. Piquet, Experimental electrical network for aircraft application, in: *IEEE VPPC Conference*, Lille, 2010, pp. 1–6.
- [13] K. Rajashekara, J. Grieve, D. Daggett, Hybrid fuel cell power in aircraft: a feasibility study for onboard power generation using a combination of solid oxide fuel cells and gas turbines, *IEEE Industry Application Magazine* 14 (3) (2008) 54–60.
- [14] X. Roboam, O. Langlois, H. Piquet, B. Morin, C. Turpin, Hybrid power generation system for aircraft electrical emergency network, *IET Electrical Systems in Transportation* 1 (4) (2011) 148–155.
- [15] X. Roboam, New trends and challenges of electrical networks embedded in more electrical aircraft, in: *ISIE, IEEE International Symposium on Gdansk*, 2011, pp. 26–31.
- [16] J.A. Rosero, J.A. Ortega, E. Aldabas, L. Romeral, Moving towards a more electric aircraft, *IEEE Aerospace and Electronic System Magazine* 22 (3) (2007) 3–9.
- [17] L. Rubino, B. Guida, P. Marino, A. Cavallo, On the selection of optimal turn ratio for transformers in isolated DC/DC boost full bridge converter, in: *SPEEDAM, International Symposium on Pisa*, 2010, pp. 39–43.
- [18] M. Sippola, R.E. Sepponen, Accurate prediction of high frequency power transformer losses and temperature rise, *IEEE Transactions on Power Electronics* 17 (5) (2002) 835–847.
- [19] T. Wu, S.V. Bozhko, G.M. Asher, D.W.P. Thomas, Accelerated functional modeling of aircraft electrical power systems including fault scenarios, in: *IECON, 35th Annual Conference of IEEE*, 2009, pp. 2537–2544.